

Frequency linewidth and decay length of spin waves in curved magnetic membranes

J. A. Otálora,^{1, a)} A. Kákay,² J. Lindner,² H. Schultheiss,² A. Thomas,¹ J. Fassbender,² and K. Nielsch^{1, 3}

¹⁾*Institute of Metallic Materials at the Leibniz Institute for Solid State and Materials Research, IFW, 01069 Dresden, Germany*

²⁾*Helmholtz-Zentrum Dresden - Rossendorf, Institute of Ion Beam Physics and Materials Research, Bautzner Landstr. 400, 01328 Dresden, Germany*

³⁾*Technische Universität Dresden, Institute of Materials Science, 01062 Dresden, Germany*

(Dated: 27 April 2022)

The curvature of a magnetic membrane was presented as a means of inducing nonreciprocities in the spin-wave (SW) dispersion relation (see [Otálora *et al. Phys. Rev. Lett.*, 2016 **117**, 227203] and [Otálora *et al. Phys. Rev. B.*, 2017 **95**, 184415]), thereby expanding the toolbox for controlling SWs. In this paper, we further complement this toolbox by analytically showing that the membrane curvature is also manifested in the absorption of SWs, leading to a difference in the frequency linewidth (or lifetime) of counterpropagating magnons. Herein, we studied the nanotubular case, predicting changes of approximately greater than 10% and up to 20% in the frequency linewidth of counterpropagating SWs for a wide range of nanotube radii ranging from 30 nm to 260 nm and with a thickness of 10 nm. These percentages are comparable to those that can be extracted from experiments on heavy metal/magnetic metal sandwiches, wherein linewidth asymmetry results from an interfacial Dzyaloshinskii-Moriya interaction (DMI). We also show that the interplay between the frequency linewidth and group velocity leads to asymmetries in the SW decay length, presenting changes between 10% and 22% for counterpropagating SWs in the frequency range of 2 - 10 GHz. For the case of the SW dispersion relation, the predicted effects are identified as the classical dipole-dipole interaction, and the analytical expression of the frequency linewidth has the same mathematical form as in thin films with the DMI. Furthermore, we present limiting cases of a tubular geometry with negligible curvature such that our analytical model converges to the case of a planar thin film known from the literature. Our findings represent a step forward toward the realization of three-dimensional curvilinear magnonic devices.

I. INTRODUCTION

In Magnonics, spin waves (SWs) or magnons – the eigenoscillations of an electron spin system¹ – are considered to be the elemental information carriers. Since magnons can propagate up to terahertz (THz) frequencies with nanometric wavelengths and over macroscopic distances without electron charges being displaced, applications based on magnons could be exempt from Joule heating, thus paving the way toward applications with unprecedentedly low power consumption (energy-friendly environmental devices), reconfigurable functionality, faster operation and further miniaturization. Remarkable progress has been achieved both theoretically and experimentally, leading to advances in the circuitry of magnonic chips, for instance, in reconfigurable waveguides for on-demand control of SWs^{2,3}, and consequently in prototype building blocks of SW-based logic elements.⁴⁻⁸

From a technological perspective, a desirable feature of magnons is the nonreciprocal (or asymmetric) dispersion relation. For instance, in SW-based logic devices, the asymmetric dispersion relation provides the condition for the unidirectional propagation of SW packages

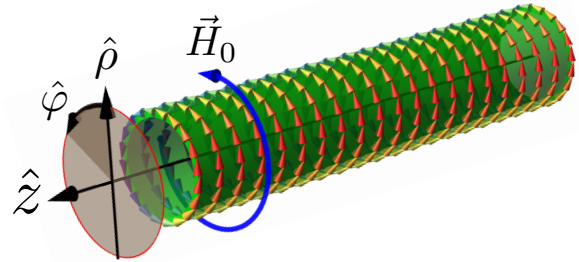


FIG. 1. (Color online). Schematic representation of a nanotube in a circular (vortex) magnetic configuration $\vec{M} = M_s \hat{\varphi}$. For nanotubes with radii smaller than a critical radius, a circular (azimuthal) magnetic field $\vec{H}_0 = H_0 \hat{\varphi}$ is required to stabilize this configuration, while the exchange interaction prefers the homogeneous magnetization state along the long axis. The critical magnetic field related to the critical radius can be analytically calculated for a nanotube with specific geometrical and material parameters, as given by Otálora *et al.*⁹. However, for radii above 100 nm, for most of the metallic magnetic materials, the vortex state is the preferred equilibrium configuration.

^{a)}Corresponding author: j.otalora@ifw-dresden.de

(avoiding the formation of standing SWs), which is fun-

damental for enhancing the input/output information transfer efficiency encoded in the phase, frequency and amplitude of SWs in the magnonic device. An asymmetric dispersion relation generally refers to the broken parity symmetry of the eigenfrequency f regarding the wavevector \vec{k} , i.e., $f[\vec{k}] \neq f[-\vec{k}]$, meaning that counter-propagating SWs with the same wavevector have different oscillation frequencies. Furthermore, a nonreciprocal dispersion relation also means an asymmetric group velocity ($\vec{v}_g \equiv 2\pi\nabla_{\vec{k}}f$). This is generally accompanied by asymmetries in lifetimes ($\tau \equiv 1/\Gamma[\vec{k}]$) and decay lengths ($l_D \equiv v_g\tau$), which are also desired properties in the pursuit of enhancing performance in SW-based communications and logic device applications.^{10,11}

Substantial efforts to enhance nonreciprocities on SWs are currently taking place, mostly in two-dimensional (2D) thin films. For instance, efforts have focused on optimizing the ferromagnetic/heavy metal interface to strengthen the Dzyaloshinskii-Moriya interaction (DMI)^{12,13} and therefore optimize the asymmetries in frequency and linewidth.^{14–18} Recently, a nonreciprocal dispersion relation was predicted by turning an ordinary 2D magnetic thin film into a curvilinear three-dimensional (3D) shape, particularly into helicoids and nanotubes. It has been predicted that the topological curvature of the 3D film induces asymmetries in the SW dispersion relation, which arises from exchange interactions in helicoids and dipole-dipole interactions in nanotubes.^{19–23} It would be expected that the membrane curvature can also induce asymmetries in the frequency linewidth and decay length of SWs; nevertheless, these features have not yet been investigated, and this paper aims to fill this gap.

Accordingly, an analytical derivation of the Polder tensor²⁴ (also known as the dynamic susceptibility tensor) of the asymmetries in the frequency linewidth and decay length and the analysis of the role of curvature are presented here only for the nanotubular geometry. As reported in previous works, the mean curvature of the nanotube breaks the chiral degeneracy of the dynamic dipolar field created by the spatial distribution of the counterpropagating SWs^{22,23} and results in the asymmetric dispersion relation. We extend our calculation to show that, as expected, curvature-induced asymmetries in frequency linewidth and decay length also occur as a consequence of such a broken chiral degeneracy.

With the aim of clearly presenting our results, the remainder of this paper is organized as follows. The analytical model is introduced in Sec. II, wherein explicit expressions for the Polder tensor, absorption, frequency linewidth, decay length and its asymmetries are obtained. These quantities are presented in Sec. III and discussed in Sec. IV. Furthermore, for completeness, a few limiting cases showing a direct resemblance with SWs in 2D thin films are shown and discussed in Sec. V. Finally, conclusions are presented in Sec. VI

II. ANALYTICAL MODEL

The nonreciprocal SW dispersion induced by curvature in cylindrical magnonic waveguides has been reported in our previous papers^{22,23}, wherein an analytical formula for the dispersion relation of SWs was presented for the case of a nanotube in an equilibrium circular (vortex) magnetic configuration. Fig. 1 illustrates the circular equilibrium state and the cylindrical coordinate system defined by the radial $\hat{\rho}$, azimuthal $\hat{\varphi}$ and longitudinal \hat{z} unitary vectors. Using these coordinates, the vortex configuration is described by $\vec{\Omega}_0 = \vec{M}/M_s = \hat{\varphi}$, the unitary magnetization field vector, and M_s , the saturation magnetization. This equilibrium magnetization and the cylindrical coordinate system will be assumed throughout the manuscript. In the following, the methods applied in our previous papers will be extended for analytically calculating the dynamic susceptibility (\aleph) and frequency linewidth (Γ) in the presence of damping. In both quantities, the curvature-induced nonreciprocity is present. The SW properties are studied by linearizing the Landau-Lifshitz Gilbert (LLG) equation of motion,

$$\dot{\vec{\Omega}} = -\gamma_0 \vec{\Omega} \times (\vec{H}_{\text{eff}} + \vec{h}_{\text{rf}}) - \alpha_G (\dot{\vec{\Omega}} \times \vec{\Omega}), \quad (1)$$

where $\gamma_0 = g\mu_B/\hbar$ is the gyromagnetic ratio, g is the electron's Landé factor, μ_B is the Bohr magneton and \hbar is the Planck constant. The effective field $\vec{H}_{\text{eff}} = \vec{H}_{\text{ex}} + \vec{H}_{\text{d}} + \vec{H}_0$ is given by the contributions of (i) the exchange field $\vec{H}_{\text{ex}} = D\nabla^2\vec{\Omega}$, where $D = l_{\text{ex}}^2 M_s$, the exchange length $l_{\text{ex}} = \sqrt{A/K_d}$, the stiffness constant A , and $K_d = (1/2)\mu_0 M_s^2$; (ii) the dipolar field $\vec{H}_{\text{d}} = -\nabla\Phi$ arising from the magnetostatic potential Φ ; and (iii) the circular (or azimuthal) $\vec{H}_0 = H_0\hat{\varphi}$ applied external magnetic field. The first term on the right side in Eq. 1, known as the Landau-Lifshitz torque, describes the precession of the magnetization in the effective field. SWs are excited with a radio-frequency magnetic field \vec{h}_{rf} . The second term on the right side in Eq. 1 is known as the Gilbert torque, where α_G is the Gilbert damping constant accounting for the relaxation mechanism that dissipates energy.

The LLG equation is linearized in terms of small perturbations of the equilibrium magnetization. Accordingly, a slightly different magnetization state $\vec{\Omega} \approx \vec{\Omega}_0 + \vec{m}$ is considered, where the radio-frequency field amplitude is assumed to be small ($\|\vec{h}_{\text{rf}}\|/M_s \ll 1$) and \vec{m} is the dynamic perturbation ($\|\vec{m}\| \ll 1$) perpendicular to the equilibrium state ($\vec{\Omega}_0 \cdot \vec{m} = 0$). The small magnetic deviation can be expressed as $\vec{m} = m_\rho\hat{\rho} + m_z\hat{z}$, and by following procedures similar to those in J. Otálora et al.^{22,23}, the dynamic equation is calculated as:

$$\begin{aligned}
\frac{\dot{m}_\rho}{\omega_{M_s}} &= -l_{ex}^2 \left(\frac{1}{b^2} + \nabla^2 \right) m_z + \frac{H_0}{M_s} m_z + \frac{\langle h_d \rangle_z}{M_s} \\
&\quad + \frac{\langle h_{rf} \rangle_z}{M_s} + \alpha_G \dot{m}_z, \\
\frac{\dot{m}_z}{\omega_{M_s}} &= l_{ex}^2 \nabla^2 m_\rho - \frac{H_0}{M_s} m_\rho + \frac{\langle h_d \rangle_\rho}{M_s} + \frac{\langle h_{rf} \rangle_\rho}{M_s} - \alpha_G \dot{m}_\rho,
\end{aligned} \tag{2}$$

where $\omega_{M_s} \equiv \gamma_0 \mu_0 M_s$, $b^{-2} = 2\pi \log(R/r)/S$, $S = \pi(R^2 - r^2)$ is the nanotube cross-section area and $\langle h_d \rangle_x = (2\pi/S) \int_r^R \rho d\rho (h_d)_x$ with $x = \rho, z$ is the cross-section average of the dynamic dipolar field components. Similarly, the radio-frequency field components are also averaged as $\langle h_{rf} \rangle_x = (2\pi/S) \int_r^R \rho d\rho (h_{rf})_x$ with $x = \rho, z$. These averages are valid for nanotubes with small thicknesses for which the dynamical magnetization components \vec{m}_ρ and \vec{m}_z are assumed to be radially invariant. Accordingly, the dynamical magnetization components in the Fourier space are written as

$$\begin{aligned}
m_\rho[\varphi, z, t] &= \sum_{n=-\infty}^{\infty} \int_{-\infty}^{\infty} dk_z e^{ik_z z} e^{in\varphi} e^{-i\omega t} \mathcal{R}_{k_z}^n, \\
m_z[\varphi, z, t] &= \sum_{n=-\infty}^{\infty} \int_{-\infty}^{\infty} dk_z e^{ik_z z} e^{in\varphi} e^{-i\omega t} \mathcal{Z}_{k_z}^n
\end{aligned} \tag{3}$$

where $\mathcal{R}_{k_z}^n$ and $\mathcal{Z}_{k_z}^n$ are the amplitude projections along the $\hat{\rho}$ and \hat{z} directions, respectively. The eigen-excitations or magnons are characterized by the longitudinal wavevector k_z along \hat{z} and by the azimuthal wavenumber (or mode) n along $\hat{\varphi}$. The averaged dipolar field can also be expanded as $\langle h_d \rangle_x = \sum_{n=-\infty}^{\infty} \int_{-\infty}^{\infty} dk_z e^{ik_z z} e^{in\varphi} e^{-i\omega t} \langle h_d \rangle_x^{n, k_z}$ with $x = \rho, z$, where $\langle h_d \rangle_x^{n, k_z}$ are the dynamic dipolar field components in the Fourier space, and their explicit form is presented in our previous work (see equation 5 in²³). Finally, the dynamic equation 2 for the excitation \vec{m} in the Fourier space can be written in the following form:

$$\begin{pmatrix} \mathcal{R}_{k_z}^n \\ \mathcal{Z}_{k_z}^n \end{pmatrix} = \aleph_{k_z}^n \begin{pmatrix} \langle h_{rf} \rangle_\rho^{n, k_z} \\ \langle h_{rf} \rangle_z^{n, k_z} \end{pmatrix} \tag{4}$$

where $\aleph_{k_z}^n$ is the dynamic susceptibility (also known as the Polder tensor²⁴), which is expressed as

$$\aleph_{k_z}^n = \begin{pmatrix} \chi_{\rho\rho}^{n, k_z} & \chi_{\rho z}^{n, k_z} \\ -\chi_{\rho z}^{n, k_z} & \chi_{zz}^{n, k_z} \end{pmatrix} = \begin{pmatrix} \frac{i\mathbb{B}}{\mathbb{A}^2 + \mathbb{B}\mathbb{C}} & \frac{i\mathbb{A}}{\mathbb{A}^2 + \mathbb{B}\mathbb{C}} \\ -\frac{i\mathbb{A}}{\mathbb{A}^2 + \mathbb{B}\mathbb{C}} & \frac{i\mathbb{C}}{\mathbb{A}^2 + \mathbb{B}\mathbb{C}} \end{pmatrix} \tag{5}$$

where $\mathbb{A} \equiv \omega - \gamma M_s \mathcal{A}_{k_z}^n$, $\mathbb{B} \equiv -\alpha_G \omega + i\omega_{M_s} \mathcal{B}_{k_z}^n$, $\mathbb{C} = -\alpha_G \omega + i\omega_{M_s} \mathcal{C}_{k_z}^n$ with $\mathcal{A}_{k_z}^n$, $\mathcal{B}_{k_z}^n$, and $\mathcal{C}_{k_z}^n$ given as

$$\begin{aligned}
\mathcal{A}_{k_z}^n &= \mathcal{K}_{k_z}^n, \\
\mathcal{B}_{k_z}^n &= l_{ex}^2 k_z^2 + (n^2 - 1)h_u + h_0 + \mathcal{L}_{k_z}^n, \\
\mathcal{C}_{k_z}^n &= l_{ex}^2 k_z^2 + n^2 h_u + h_0 + \mathcal{J}_{k_z}^n,
\end{aligned} \tag{6}$$

where the term $h_u = H_u/M_s = l_{ex}^2/b^2 \geq 0$ is the exchange field arising from the vortex state of the magnetization. This field can be viewed as a shape anisotropy with the large nanotube axis \hat{z} as the easy axis. The terms denoted by $\mathcal{J}_{k_z}^n$, $\mathcal{K}_{k_z}^n$ and $\mathcal{L}_{k_z}^n$ are hypergeometrical functions that depend on the nanotube radius R and thickness d , and their explicit formulations (the detailed derivation is presented in²³) are

$$\begin{aligned}
\mathcal{J}_{k_z}^n &= \frac{\pi}{S} \int_0^\infty dq \frac{q^3}{2(q^2 + k_z^2)} (\Gamma_n[q])^2 \\
\mathcal{K}_{k_z}^n &= \frac{\pi}{S} \int_0^\infty dq \frac{q^2 k_z}{q^2 + k_z^2} \Gamma_n(q) \Lambda_n[q] \\
\mathcal{L}_{k_z}^n &= \frac{\pi}{S} \int_0^\infty dq \frac{2q k_z^2}{q^2 + k_z^2} (\Lambda_n[q])^2
\end{aligned} \tag{7}$$

with $\Lambda_n[q] = \int_r^R d\rho \rho J_n[q\rho]$, $\Gamma_n[q] = \Lambda_{n-1}[q] - \Lambda_{n+1}[q]$, and $J_n[x]$ the first kind Bessel functions of order n .

Note that the term $\mathcal{A}_{k_z}^n$ emerges only from the dynamic dipolar fields induced by the nanotubes' curvature and vanishes for planar films. As shown in our previous works^{22,23}, this term is the origin for the asymmetric dispersion relation and will play the same role in frequency linewidth. Moreover, note that $\mathcal{A}_{k_z}^n$, $\mathcal{B}_{k_z}^n$ and $\mathcal{C}_{k_z}^n$ are the normalized stiffness fields consisting of dynamic and static components of the exchange, magnetostatic and external fields. These features will be discussed later in section IV, *Discussions*.

The SW absorption (or dynamical susceptibility) can be expressed in the following Lorentzian form by using the Polder tensor defined in Eq. 5 as $\mathcal{S}_{\rho\rho}^{n, k_z}(\omega) = \text{Im}(\aleph_{\rho\rho}^{n, k_z})$

$$\mathcal{S}_{\rho\rho}^{n, k_z}[\omega] = \frac{\mathcal{W}_{k_z}^n[\omega, \alpha_G]}{(\omega^2 - (\omega_{k_z}^n)^2)^2 + (\frac{1}{2}\Delta_{k_z}^n[\omega])^2} \tag{8}$$

where the eigenfrequency $\omega_{k_z}^n$ and the terms $\Delta_{k_z}^n(\omega)$ and $\mathcal{W}_{k_z}^n(\omega, \alpha_G)$ are given as

$$\omega_{k_z}^n = \omega_{M_s} \left(\mathcal{A}_{k_z}^n + \sqrt{\mathcal{C}_{k_z}^n \mathcal{B}_{k_z}^n} \right), \tag{9}$$

$$\Delta_{k_z}^n[\omega] = 2\omega_{M_s} \alpha_G \omega \left(\mathcal{C}_{k_z}^n + \mathcal{B}_{k_z}^n \right) \left(\frac{\omega + \omega_{k_z}^n}{\omega - \bar{\omega}_{k_z}^n} \right) \tag{10}$$

and

$$\begin{aligned}
\mathcal{W}_{k_z}^n &= -\frac{(\omega + \omega_{k_z}^n)}{(\omega - \bar{\omega}_{k_z}^n)} \left(\alpha_G \omega_{M_s} \omega \left(\omega^2 - (\omega_{k_z}^n)^2 \right) \right. \\
&\quad \left. + \frac{(\omega_{M_s})^2}{2} \Delta_{k_z}^n \mathcal{B}_{k_z}^n \right),
\end{aligned} \tag{11}$$

with $\bar{\omega}_{k_z}^n = \omega_{M_s} (\mathcal{A}_{k_z}^n - \sqrt{\mathcal{C}_{k_z}^n \mathcal{B}_z^n})$. For planar thin films, the term $\mathcal{A}_{k_z}^n$ vanishes, and equation 9 simplifies to the dispersion relation that is well known from the literature.^{22,23} The analytical expression for the group velocity can be obtained from the k_z -derivative of the eigenfrequency, $v_g[n, k_z] = \partial \omega_{k_z}^n / \partial k_z$, and the frequency linewidth Γ can be obtained from the absorption equation 8. Note that the Lorentzian susceptibility should be inversely proportional to the linewidth as a quadratic term, i.e., $\mathcal{S}_{\rho\rho}^{n, k_z}[\omega] \propto ((\omega - \omega_{k_z}^n)^2 - (\Gamma/2)^2)^{-1}$. Hence, from equations 8 and 10, (when $\Delta_{k_z}^n[\omega] / (\omega + \omega_{k_z}^n)$ is evaluated for the eigenfrequencies $\omega = \omega_{k_z}^n$), it is straightforward to deduce the equation of the frequency linewidth as follows:

$$\Gamma[n, k_z] = \omega_{M_s} \alpha_G (\mathcal{C}_{k_z}^n + \mathcal{B}_{k_z}^n) \left(1 + \frac{\mathcal{A}_{k_z}^n}{\sqrt{\mathcal{B}_{k_z}^n \mathcal{C}_{k_z}^n}} \right) \quad (12)$$

This expression reduces to that of the frequency linewidth of 2D thin films when the nanotube radius goes to infinity ($\mathcal{A}_{k_z}^n = 0$). In this case, the linewidth directly depends on the stiffness fields and the Gilbert damping parameter as well known from the literature^{17,25–28}. For nanotubes with finite radii, equation 12 takes a similar mathematical form as that derived for planar 2D heavy metal/magnetic metal sandwiches with interfacial DMI (see equation 8 in¹⁷). The asymmetries in Γ are introduced by the broken mirror symmetry of $\mathcal{A}_{k_z}^n$, i.e., $\mathcal{A}_{k_z}^n = -\mathcal{A}_{-k_z}^n$, which is the same term giving the asymmetries of the dispersion relation in nanotubes (see equation 9 and equations 6 and 10 in²³). This term arises from the broken mirror symmetry of the dynamic dipolar field, which can be understood from the role of the mean curvature of the nanotube ($1/\bar{\rho} = 2/(R+r)$) in breaking the mirror symmetry of the dynamic magnetic charges that create the dynamic dipolar field. Here, R and r are the outer and inner radii of a nanotube, respectively. The asymmetry on the volume charges was previously used to explain the curvature-induced asymmetric dispersion relation in nanotubes^{22,23} and will be used again in the section IV, *Discussions*, to explain the asymmetries in the frequency linewidth in more detail.

The frequency linewidth asymmetry can be defined as $\Delta\Gamma[n, k_z] \equiv |\Gamma[n, k_z] - \Gamma[n, -k_z]|$ and has the form of

$$\Delta\Gamma[n, k_z] = 2\omega_{M_s} \alpha_G |\mathcal{C}_{k_z}^n + \mathcal{B}_{k_z}^n| \frac{|\mathcal{A}_{k_z}^n|}{\sqrt{\mathcal{B}_{k_z}^n \mathcal{C}_{k_z}^n}} \quad (13)$$

Note that the frequency linewidth asymmetry is zero ($\Delta\Gamma[n, k_z] = 0$) for $k_z = 0$ as a consequence of the odd parity of $\mathcal{A}_{k_z}^n$. The results of the frequency linewidth and its asymmetry will be presented in the next section III, *Results*.

III. RESULTS

In the following, the results of the analytical model are presented assuming a permalloy nanotube with outer (inner) radius $R = 80$ nm ($r = 70$ nm), saturation magnetization $\mu_0 M_s = 1$ T, exchange stiffness constant $A = 13$ pJ/m and exchange length $l_{\text{ex}} \approx 5.8$ nm. The preferred equilibrium state for these material parameters and geometrical dimension in the absence of external fields is the saturated state along the long axis of the nanotube. The critical field to stabilize the vortex magnetic state is calculated to be $\mu_0 H_{\text{crit}} = \mu_0 H_u \approx 5.9$ mT.⁹ Therefore, a field of $\mu_0 H_0 = 6$ mT is applied to set the circular magnetization state.

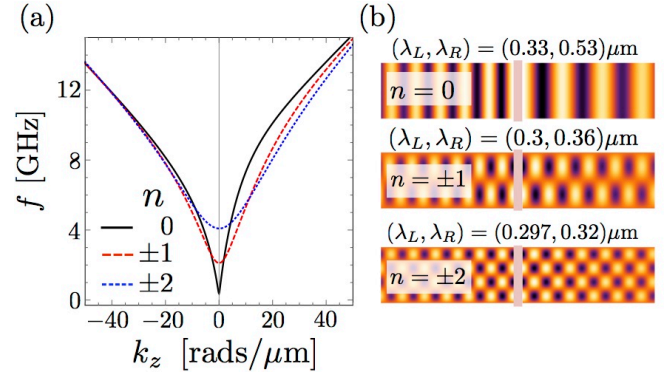


FIG. 2. (Color online). (a) Eigenfrequency and (b) radial component of SW distribution in an unrolled view of the nanotube at an oscillation frequency of 8 GHz. λ_L and λ_R correspond to the left (L) and right (R) wavelengths of counter-propagating SWs, respectively. An infinitely large permalloy nanotube of outer (inner) radius $R = 80$ nm ($r = 70$ nm) and under the action of an azimuthal field $\mu_0 H_0 = 6$ mT is assumed. Curves are presented for the azimuthal wavenumbers $n = 0, \pm 1, \pm 2$.

Figure 2 summarizes our results for SWs with the zeroth-order and the first two higher-order modes in terms of the azimuthal wavenumbers $n = 0, \pm 1, \pm 2$. The dispersion relation $f[n, k_z] = \omega_{k_z}^n / (2\pi)$ is shown in figure 2a). The asymmetry of the dispersion relation is mostly pronounced for the zeroth-order modes, as shown in our previous works^{22,23}. The mode profiles in an unrolled view of the tube are displayed in figure 2b), where the color code encodes the radial component of the magnetization. These modes excited with an RF field of 8 GHz in the middle of the nanotube (marked with a pink shadowed region) are planar waves with no nodal line for $n = 0$, two nodal lines for $n = \pm 1$ and four nodal lines for $n = \pm 2$. The left and right wavelengths of the counterpropagating waves are denoted as λ_L and λ_R , respectively.

The frequency linewidth Γ scaled by the Gilbert damping α_G as a function of the SW wavevector k_z and of the eigenfrequency is shown in Figure 3(a) and (b), respectively. The linewidth is asymmetric for the modes with

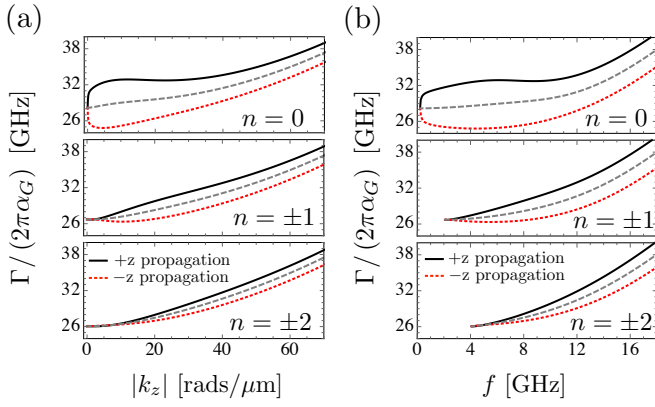


FIG. 3. (Color online). Role of curvature in the frequency linewidth of a magnetic nanotube and comparison with the frequency linewidth of a 2D thin film. The frequency linewidth as functions of (a) wavevector k_z and (b) eigenfrequency f . Curves are presented for the azimuthal wavenumbers $n = 0, \pm 1, \pm 2$. The black continuous and red dotted lines correspond to the frequency linewidth as a function of counterpropagating SWs in an infinitely large permalloy nanotube of outer (inner) radius $R = 80$ nm ($r = 70$ nm) and under the action of an azimuthal field $\mu_0 H_0 = 6$ mT. The gray dashed lines correspond to the case of an extended 2D thin film with a 10 nm thickness and with an in-plane magnetization oriented parallel to the magnetic field $\mu_0 H_0 = 6$ mT. The 2D thin film is assumed to have an in-plane hard axis oriented perpendicularly to $\mu_0 H_0$ and represented by the anisotropic field $\mu_0 H_u = 5.9$ mT. The Gilbert damping parameter is denoted by α_G . The 2D thin film is supposed to resemble the unrolled view of the nanotubular configuration. The SW wavenumbers k_z and n in the nanotube correspond to the wavevectors $k_Z = n/\bar{\rho}$ and $k_X = k_z$ in the thin film, respectively. Therefore, with $\bar{\rho} = (R + r)/2 = 75$ nm, the wavevectors k_Z corresponding to $n = 0, \pm 1, \pm 2$ are $k_Z = 0, \pm 1/75, \pm 2/75$ nm.

the same wavevector magnitude (see Figure 3(a)), same eigenfrequency (see Figure 3(b)) and opposite propagation directions. The influence of the nanotube curvature on the frequency linewidth can be better understood by comparing it with the limiting case of a noncurved membrane, which consists of a planar thin film. In this comparison, we consider a planar permalloy thin film with a magnetic configuration similar to that in the unrolled view of the nanotube. Therefore, an extended 2D thin film is assumed with an in-plane applied magnetic field H_0 parallel to the homogeneous (in-plane) equilibrium magnetization $\vec{\Omega}_0$, thickness d , and easy-axis anisotropy characterized by the field H_u and perpendicular to $\vec{\Omega}_0$. In figure 3, we plot with gray dashed lines the frequency linewidth for the planar permalloy thin film, and we plot with black solid and red dotted lines the linewidth for counterpropagating SWs in the NT. These curves are analyzed and discussed in the next section, *Discussions*. Note that the range of Γ values predicted by our analytical calculations is consistent with the values measured experimentally for permalloy^{29,30}. Indeed, assuming typi-

cal values for the Gilbert damping parameter α_G between 0.001 and 0.01, one can observe the frequency linewidth ranging between 200 and 300 MHz for the given range of eigenfrequencies and wavevectors.

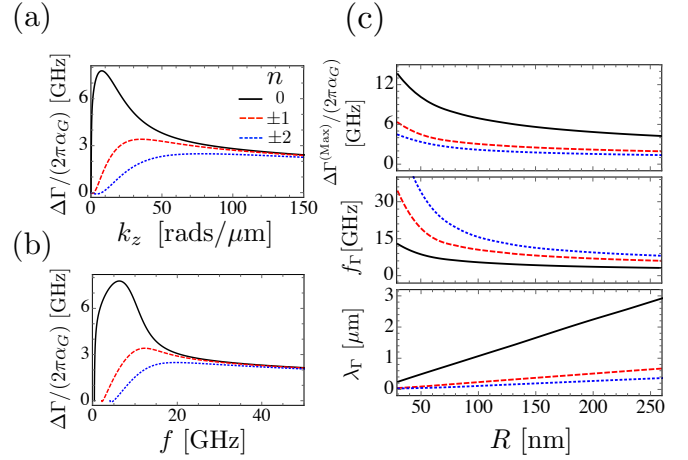


FIG. 4. (Color online). Frequency linewidth asymmetries (defined by equation 13) at the fundamental $n = 0$ (black lines) and at the first two higher-order azimuthal modes $n = \pm 1$ (red dashed line) and $n = \pm 2$ (blue dotted line). Evolution of the frequency linewidth asymmetry as a function of (a) the wavevector k_z and (b) eigenfrequency of SWs. (c) Radial dependence of the maximum linewidth asymmetry $\Delta\Gamma^{(\text{Max})}$ (upper curve), of the wavelength λ_Γ (middle curve) and of the eigenfrequency f_Γ (bottom figure) of SWs at which the asymmetry reaches its maximum. All cases presented here are calculated for the nanotube thickness $d = 10$ nm. An infinitely large nanotube with outer radius $R = 80$ nm and an applied circular field of $\mu_0 H_0 = 6$ mT are assumed in (a) and (b). An applied circular field slightly larger than the critical field ($H_0 = 1.01H_c$)⁹ is assumed for calculating the curves in (c).

The linewidth asymmetry $\Delta\Gamma$, defined as the difference in the linewidth between counterpropagating SWs with the same wavevector magnitude and eigenfrequency, are shown in Figure 4 (a) and (b), respectively. As shown, in all modes, $\Delta\Gamma$ shows a maximum defined as $\Delta\Gamma^{(\text{Max})}$, which occurs at a particular frequency ($f = f_\Gamma$) and wavevector ($k_z = k_\Gamma$). The evolution of the quantities $\Delta\Gamma^{(\text{Max})}$, f_Γ and $\lambda_\Gamma = 2\pi/k_\Gamma$ as a function of the NT radius is summarized in Figure 4(c). The linear relation between λ_Γ and R indicates that the asymmetry is induced by the nanotube mean curvature ($\sim 1/R$). (Note that in the case of the asymmetry in the dispersion relation, a global maximum located at λ_{SW} is also found, showing a similar relation with the nanotube mean curvature ($\sim 1/R$).^{22,23}) The changes in the linewidth asymmetries between counterpropagating SWs can be estimated by comparing the values of $\Delta\Gamma^{(\text{Max})}$ in figure 4(c) with the values for Γ in figure 3. Indeed, changes of approximately greater than 10% and up to 20% for a wide range of nanotube radii between 30 nm and 260 nm are observed, which is comparable with those that can be extracted

from experiments on heavy metal/magnetic metal sandwiches wherein linewidth asymmetry results from interfacial DMI.¹⁷

The SW decay length, $l_D[n, k_z] \equiv v_g[n, k_z]/\Gamma[n, k_z]$, and the decay length asymmetry $\Delta l_D[n, k_z] = l_D[n, k_z] - l_D[n, -k_z]$ in the nanotubular membrane are shown in figure 5. Here, the group velocity is given by the derivative $v_g[n, k_z] \equiv d\omega_{k_z}^n/dk_z$. From figure 5 (a) and (b), we can observe changes ranging between 10% and 22% in the decay length in the range of frequencies between 2 GHz and 10 GHz and for three different nanotube radii (these changes are estimated by $\Delta l_D[n, k_z]/l_D[n, k_z]$). Note that the percentage differences are approximately 20% for $n = 0$ and frequencies between 4 GHz and 6 GHz in the case of a nanotube with $R = 80$ nm. Moreover, similar values are also found for the larger nanotube radius $R = 300$ nm at the frequency range of 2 - 3 GHz. For larger modes ($n \neq 0$), the percentage difference decreases to approximately 13% due to the reduced curvature-induced asymmetry of group velocity v_g (the larger is the mode number, the smaller is the difference between the slope of the dispersion relation of counterpropagating SWs) and linewidth Γ (reduction of the asymmetries in Γ at larger-order mode numbers are explained in the next section). Note that the range of frequencies at which the asymmetries are more evident corresponds to the magneto-chiral dipolar effect induced by the mean nanotube curvature; therefore, it is observed to be more intense around wavevectors $k_z \sim 1/R$.

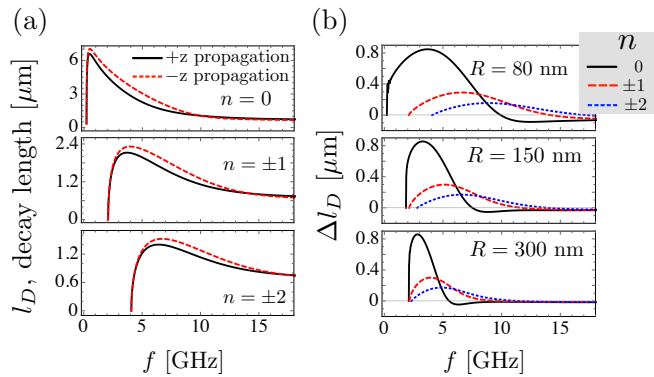


FIG. 5. (Color online). Decay length of counterpropagating SWs (a) and decay length asymmetries (b) as a function of SW eigenfrequency and for wavenumber $n = 0, \pm 1, \pm 2$. An infinitely large nanotube with outer radius $R = 80$ nm, inner radius $r = 70$ nm, in a vortex-oriented equilibrium magnetization $\vec{M}_0 = M_s \hat{\varphi}$ and under the action of an applied circular field $\mu_0 H_0 = 6$ mT is assumed in (a). The same circular field is assumed for calculating the curves in (b). Note that for all radii in (b), the applied circular field magnitude is larger than the critical field necessary for stabilizing the circular magnetization⁹ A Gilbert damping parameter $\alpha_G = 0.001$ for the permalloy nanotube was considered.

IV. DISCUSSIONS

The term responsible for the asymmetry of the frequency linewidth Γ (see equation 12) is $\mathcal{A}_{k_z}^n$ (originating from the dynamic dipolar field), which also gives rise to the asymmetric dispersion relation shown in Otálora *et al.*²². This result reveals that nonreciprocities in the frequency linewidth are also induced by the surface curvature.

The influence of the dynamic dipolar interaction on the linewidth can be better understood if we first discuss the analytical expressions for the thin-film case. Indeed, we present this discussion here for the purpose of completeness and self-containedness of the manuscript. We consider a 2D thin film with the equilibrium magnetic configuration, anisotropies and applied magnetic fields similar to those in the unrolled view of the assumed nanotube configuration. Accordingly, a 2D thin film with in-plane orthonormal axes \hat{X} and \hat{Z} , out-of-plane axis \hat{Y} , easy anisotropy axis represented by the field $H_u \hat{X}$, applied magnetic field $H_0 \hat{Z}$ and equilibrium magnetization $\vec{M}_0 = M_s \hat{Z}$ will be assumed. This configuration can resemble the unrolled view of the nanotube by mapping the unit vectors \hat{X} , \hat{Y} and \hat{Z} to $-\hat{z}$, $\hat{\rho}$ and $\hat{\varphi}$, respectively. As before, H_u is the exchange field arising from the vortex state of the magnetization, and H_0 is the applied circular field. The chosen notation for the unit vectors \hat{X} , \hat{Y} and \hat{Z} is intentional for a later comparison with the literature.

According to the literature,^{25–28} the frequency linewidth of an extended thin film Γ_{2D} is proportional to the sum of the stiffness fields and can be written as (the film is considered to be free of defects and perfectly smooth, and thus, two-magnon scattering is excluded)

$$\Gamma_{2D}[\vec{k}] = \omega_{M_s} \alpha_G \left(h_X[\vec{k}] + h_Y[\vec{k}] \right). \quad (14)$$

Here, $\vec{k} = k_X \hat{X} + k_Z \hat{Z}$ is the in-plane wavevector (out-of-plane wavevector components are not taken into consideration) with $k_X = k \sin \phi_k$ and $k_Z = k \cos \phi_k$ being its components, and ϕ_k is the angle between the magnetization and the wavevector.³¹ The thin-film thickness (equal to the nanotube thickness) is denoted by d , and $h_{X,Y}[\vec{k}] = H_{X,Y}[\vec{k}]/M_s$ are the normalized stiffness fields with the following form:

$$\begin{aligned} H_X[\vec{k}] &= H_0 - H_u + H_X^{\text{dip}}[|k|d, \phi_k] + M_s l_{ex}^2 k^2, \\ H_Y[\vec{k}] &= H_0 + H_Y^{\text{dip}}[|k|d] + M_s l_{ex}^2 k^2, \end{aligned} \quad (15)$$

where $H_X^{\text{dip}}[|k|d, \phi_k]$ and $H_Y^{\text{dip}}[|k|d]$ are the in-plane and out-of-plane stiffness dipolar fields given as

$$\begin{aligned} H_X^{\text{dip}}[|k|d, \phi_k] &= M_s F[|k|d] \sin^2[\phi_k], \\ H_Y^{\text{dip}}[|k|d] &= M_s (1 - F[|k|d]), \end{aligned} \quad (16)$$

with $F[|k|d] = 1 - (1 - e^{-|k|d})/(|k|d)$. Note that the wavevectors in the 2D thin film k_X and k_Z map respectively to the wavevectors k_z and \bar{k}_φ in the nanotube, where $\bar{k}_\varphi = (2\pi/S) \int_r^R k_\varphi \rho d\rho = n/\bar{\rho}$ is the radially averaged azimuthal wavevector $k_\varphi = n/\rho$ with $\bar{\rho} = (R + r)/2$ as the mean nanotube radius. Furthermore, in the nanotube, the angle ϕ_k is subtended between the circular equilibrium magnetization $\vec{\Omega}_0 = \hat{\varphi}$ and the total wavevector $\vec{k} = k_\varphi \hat{\varphi} + k_z \hat{z}$, and it is given by $\tan[\phi_k] = k_z/\bar{k}_\varphi = \bar{\rho} k_z/n$. In addition, note that by comparing equation 12 with equation 14, we realize that the quantities $\mathcal{B}_{k_z}^n$ and $\mathcal{C}_{k_z}^n$ (see equation 6) play the role of the normalized stiffness fields in the nanotube in an analogous manner to that played by $h_X[\vec{k}]$ and $h_Y[\vec{k}]$ in the planar thin film, respectively. The remaining term $\mathcal{A}_{k_z}^n$ arises from the NT curvature; hence, there is no equivalent term in the planar case unless there is a DMI interaction included, which is not the case in equation 14.

Now, from equations 14 and 15, the frequency linewidth takes the following explicit form:

$$\Gamma_{2D}[k, \phi_k] = \alpha_G \frac{\omega M_s}{M_s} (2H_0 - H_u + H_X^{\text{dip}}[|k|d, \phi_k] + H_Y^{\text{dip}}[|k|d] + 2M_s l_{ex}^2 k^2). \quad (17)$$

This equation is clearly mirror symmetric; by replacing ϕ_k with $\phi_k + \pi$, the $\Gamma_{2D}[\vec{k}] = \Gamma_{2D}[-\vec{k}]$. The frequency linewidth for the backward volume (BV) ($\Gamma_{2D,BV}$ and $k = k_Z$) and Damon-Eshbach (DE) ($\Gamma_{2D,DE}$ and $k = k_X$) geometries can be obtained for the angles $\phi_k = 0$ and $\phi_k = \pi/2$, respectively. The equations are the following:

$$\Gamma_{2D,BV} = \alpha_G \frac{\omega M_s}{M_s} (2H_0 - H_u + H_Y^{\text{dip}}[|k_Z|d] + 2M_s l_{ex}^2 k_Z^2) \quad (18)$$

$$\Gamma_{2D,DE} = \alpha_G \frac{\omega M_s}{M_s} (2H_0 - H_u + M_s + 2M_s l_{ex}^2 k_X^2). \quad (19)$$

Note that the DE and BV geometries in the nanotube can be described from the limiting cases of the intermedium SW configuration (see equation 12) that is defined by all possible values of n and k_z . Analogous with a 2D thin film described by equation 17, in the nanotube, it is easily realized that the DE geometry, $\phi_k = \pi/2$, corresponds to $n = 0$ and the BV geometry, $\phi_k = 0$, to $k_z = 0$ and $n \neq 0$, or to the limiting case $n \gg \bar{\rho} k_z$; hence, $k \approx \bar{k}_\varphi$.

In the following, we would like to focus on the contributions of H_X^{dip} and H_Y^{dip} (see equation 15) to the frequency linewidth (note that in both fields, the function $F[|k|d]$ introduces the dynamic dipolar field created by the dipolar charges of an SW with wavevector magnitude k). The field H_X^{dip} , on the one hand, is nonzero

for any angle different than zero $\phi_k \neq 0$, and it is a purely dynamic dipolar field that arises from the divergence of the magnetization (volume charges) when an SW is traveling along the X direction. The field H_Y^{dip} , on the other hand, is given by the addition of two terms: the static out-of-plane demagnetizing field of an infinite 2D film, M_s (the demagnetizing tensor component $N_Y = 1$) and the dynamic field, $-M_s F[|k|d]$, created by the redistribution of surface charges due to the excited SW. For $k = 0$, the ferromagnetic resonance case (FMR), the $F[|k|d] = 0$; therefore, the in-plane component is zero $H_X^{\text{dip}} = 0$, and the out-of-plane field is equal to the static demagnetizing field, $H_Y^{\text{dip}} = M_s$. For nonzero wavevectors, the field H_X^{dip} depends on the angle φ_k , and the out-of-plane component H_Y^{dip} is reduced by the surface-charge-induced dynamic dipolar field, $-M_s F[|k|d]$. The consequences of H_X^{dip} and H_Y^{dip} (therefore, the role of the dynamic dipolar charges) in the frequency linewidth at the BV, DE and intermedium configurations in a planar thin-film is presented next.

In the BV configuration ($\phi_k = 0$), only the surface dynamic dipolar charges and the out-of-plane field component are nonzero. Consequently, the frequency linewidth will present a dipolar-dominated regime that is introduced by the surface charges via H_Y^{dip} . This results in a decreasing linear dependence on k_Z , which is dominant at small wavevector values in $k = k_Z \ll 1/d$ (long-wavelength SWs). However, above a critical wavevector, the exchange field will dominate, and an increasing dependence on k_Z^2 is presented. (Note that a similar resemblance in k_Z can be found in the BV dispersion relation).

In the intermedium configuration ($0 < \phi_k < \pi/2$), the volume dynamic dipolar field H_X^{dip} is reduced by a factor of $\sin[\phi_k]^2$; therefore, at a small wavevector magnitude $k \ll 1/d$, the dynamic dipolar contribution from surface charges will dominate on the frequency linewidth (equation 17). Therefore, in a similar fashion as in the BV geometry, the frequency linewidth here will present a decreasing linear dependence on k , but in a shorter range of wavevector magnitude. This situation can be slightly observed by the gray dashed curve in figure 3(a) for $n = \pm 1$ at $k_z < 3$ rads/ μm (or $k < 3$ rads/ μm) and for $n = \pm 2$ at $k_z < 5$ rads/ μm (or $k < 5$ rads/ μm).

In the DE configuration ($\phi_k = \pi/2$), the dynamic dipolar fields from both the in-plane and out-of-plane stiffness dipolar fields cancel each other, which is due to the additive contribution of both fields to the linewidth (see equation 19). Here, the dynamic surface and volume charges induce in H_Y^{dip} and H_X^{dip} the same magnitude (but opposite in sign) dynamic dipolar fields ($M_s F[k_X d]$); hence, the term $M_s F[k_X d]$ in the linewidth cancels out. This means that the effects of volume and surface charges compensate each other, and the dipolar contribution in the frequency linewidth turns into a constant given by the full demagnetizing field (M_s). Consequently, in the DE geometry, the wavevector dependence of the linewidth is only driven by the exchange interaction, leading to a

k_X^2 behavior, as indicated by the gray dashed line in figure 3(a) for $n = 0$ (or $k_z = 0$).

Note that whether a DE, BV or intermedium configuration, a linear relation between the frequency linewidth and SW frequency is generally expected. According to equation 17, this can be observed at frequency values where the exchange interaction dominates over the dipolar, shape H_u and Zeeman H_0 contributions. Under this condition, the SW frequency and linewidth approximate to $f \approx (\omega_{M_s}/2\pi)l_{ex}^2 k^2$ and $\Gamma_{2D} \approx 2\alpha_G \omega_{M_s} l_{ex}^2 k^2$, respectively. These two equations lead to $\Gamma_{2D} \approx 4\pi\alpha_G f$, which can be observed by the gray dashed line but at larger frequencies than presented in figure 3(b) for $n = 0, \pm 1, \pm 2$.

At this point, we will continue with the analysis of the frequency linewidth equation 12 of the magnetic nanotube. We will utilize the aforementioned SW configurations at the 2D thin film for our next developments. In the following, the discussion of the frequency linewidth in the tubular membrane will be separated into two subsections: one corresponding to the DE configuration ($n = 0$) and the other corresponding to the intermedium configuration ($n \neq 0$) that includes the BV geometry at the limit $n \gg \bar{\rho}k_z$.

A. Linewidth in DE configuration ($n = 0$)

As previously mentioned, the asymmetries in the frequency linewidth are given by $\mathcal{A}_{k_z}^n$. This term is linear in k_z with a positive slope for wavevector values up to $k_z \sim 1/R$. The term $\mathcal{A}_{k_z}^n$ is responsible for the differences in the linewidth between the nanotube and the 2D thin film at the DE configuration: in the nanotube for SWs traveling with $k_z > 0$ (+ z propagation), the linewidth increases linearly, and for the oppositely propagating SWs $k_z < 0$ (- z propagation), the linewidth decreases linearly. These features are observed in figure 3(a) for $n = 0$ and $|k_z| < 4 \text{ rads}/\mu\text{m}^{-1}$. A similar linear behavior between the frequency linewidth and eigenfrequency of counterpropagating SWs at $f < 1 \text{ GHz}$ can also be observed in figure 3(b). This result can be understood from the first-order expansion of the eigenfrequency in terms of the wavevector, $f = f_0 + \nu_0 k_z$, where ν_0 is a constant slope that depends on the nanotube radius and f_0 is the nanotube ferromagnetic resonance - FMR.²³ Since $\Gamma[n = 0, k_z]$ and f are linear in k_z at first-order expansion, Γ is also linear in f at the same expansion order. From this linear relation, the not mirror symmetry of the frequency linewidth $\Gamma[n = 0, k_z] \neq \Gamma[n = 0, -k_z]$ is clearly realized. The linewidth asymmetry with a decreasing tendency can also be obtained at the exchange-dominated regime: in the range $k_z \gg 1/R$, the asymmetry will eventually be neglected for sufficiently large k_z . Moreover, as in the 2D thin film, in the nanotube, the exchange-dominated frequency linewidth is also linear in the eigenfrequency f , a situation that can be obtained at larger frequencies than presented in figure 3(b)

The frequency linewidth asymmetry mentioned above

can be understood in terms of the dynamic dipolar field created by the dynamic dipolar charges. In contrast to the preserved mirror symmetry of dipolar charges in 2D thin films, in the nanotube, the symmetry is disturbed by the tubular mean curvature. In the nanotube, the surface charges conserve the mirror symmetry, and the magnitude of the volume charges violate it.²² This breaks the mirror symmetry of the dynamic dipolar fields and consequently violates the left-right chiral symmetry of the frequency linewidth of counterpropagating SWs. On the one hand, for $k_z < 0$, the divergence of the dynamic magnetization and the strength of the volume dynamic dipolar field are reduced. Hence, the field created by surface charges dominates. Understanding that the surface charges and its dynamic dipolar field strength decrease with increasing the wavevector magnitude k_z , it is found that in a first-order expansion in k_z , the frequency linewidth shows a non-negligible decreasing tendency. Note that this situation resembles a behavior similar to that in the BV geometry (or in the intermedium geometry) in 2D thin films, wherein the effects of the volume dynamic charges are absent (or reduced). On the other hand, for SWs with $k_z > 0$, the divergence of the dynamic magnetization and the volume dynamic charges are enhanced. Thus, the dynamic dipolar fields arising from the volume charges dominate over the dynamic fields from the surface charges. Realizing that the divergence of the SW distribution and the volume dynamic dipolar field increase with increasing SW wavevector, it is found that the frequency linewidth has a non-negligible linear increasing tendency with k_z . The aforementioned linear trend between Γ and k_z is reflected in figure 3(a) at small values of k_z , as previously mentioned (for comparison, note that in the 2D thin film, both dynamic fields balance each other, leading to an absent linear k_z contribution in the frequency linewidth). Finally, for a larger wavevector magnitude, the exchange interaction will eventually dominate over the dipolar interaction, and the frequency linewidth will take a k_z^2 dependence, as discussed previously. (Recall that in a 2D thin film in a DE geometry, the total dynamic dipolar field contribution to the linewidth is constant and equal to the magneto-static demagnetizing field, leading to a k_z^2 dependence in the frequency linewidth that originates from the exchange energy).

B. Linewidth in intermedium configuration ($n \neq 0$)

For higher-order modes ($n \neq 0$), the geometry of SWs is defined by the angle ϕ_k subtended between the wavevector $\vec{k} = k_z \hat{z} + \bar{k}_\varphi \hat{\varphi}$ (where $\bar{k}_\varphi = n/\bar{\rho}$) and the equilibrium magnetization $\vec{\Omega}_0$. The BV geometry, $\phi_k = \pi/2$, is characterized by the lack of asymmetries in the frequency linewidth and is given by whether doing $k_z = 0$ or in the limit of $|n| \gg \bar{\rho}|k_z| \sim R|k_z|$. As observed in figure 3(a) for $n = \pm 1, \pm 2$, the absence of asymmetries in the case of $k_z = 0$ can be understood if we take

into account that the dynamic volume charges (obtained from the divergence of the dynamic excitation - the SW) are free of curvature-induced asymmetries. Similarly, no asymmetries must also be observed in terms of the eigenfrequency f , as is indeed shown in figure 3(b) for $n = \pm 1, \pm 2$ at the eigenfrequency $f[k_z = 0]$ where all curves converge. More details about $k_z = 0$ will be presented in subsection V A. In the other BV geometry case, at the limit $|n| \gg \bar{\rho}|k_z|$, asymmetries in the frequency linewidth are not presented. For any value of k_z (large $|k_z| \gg 1/R$, small $|k_z| \ll 1/R$ or located at the optimal asymmetry $|k_z| \sim 1/R$), the integer nature of n leads to the limit $|n| \gg 0$ as the sufficient condition to define the BV geometry. For illustration, we consider the range $|k_z| \sim 1/R$. Accordingly, we obtain $\bar{\rho}|k_z| \sim 1$; therefore, $|n| \gg 1$. In terms of the azimuthal wavevector, the condition $|n| \gg 1$ means that $|k_\varphi| \gg 1/R$. Consequently, the total wavevector magnitude is $k \approx |k_\varphi| \gg 1/R$, which is located at the exchange-dominated regime that is characterized for no curvature-induced asymmetries (via dipolar interaction) in the frequency linewidth.

For finite values of n , we obtain the intermedium configuration defined by $0 < \phi_k < \pi/2$. In this case, less intense asymmetries in the frequency linewidth than with $n = 0$ appear, which is a consequence of the fact that the larger is the value of n , the more important is the exchange interaction. Figure 3 shows reduced asymmetric frequency linewidth of counterpropagating SWs for $n = \pm 1, \pm 2$ in a wide range of wavevectors k_z and eigenfrequencies f , and the asymmetries are quantified in figure 4. Since this nonreciprocal effect is curvature induced, the asymmetry $\Delta\Gamma$ must decrease (i) by increasing the wavevector k_z at $k_z > 1/R \approx 12.5$ rads/ μm (see figure 4(a)) and consequently (ii) by increasing the SW frequencies for over $f[1/R] \approx 5.6$ GHz (see figure 4(b)). These values correspond to a nanotube with $R = 80$ nm. An analytical expression of the frequency linewidth for finite n and small wavevector range $k_z \ll 1/R$ can be obtained, showing a direct resemblance with 2D thin films with DMI; nevertheless, this case is presented in subsection V C.

V. LIMITING CASES

For completeness of our comparative analysis between the 2D thin film and nanotubular membrane, a few limiting cases of the nanotube frequency linewidth are presented. In the following, we will address three cases consisting of A. $k_z = 0$, B. $k_z \gg 1/R$, and C. $k_z \neq 0$ ($k_z \ll 1/R$), in which the nanotubular curvature can be neglected; therefore, the frequency linewidth is reduced to well-known expressions for 2D films.

A. For $k_z = 0$

In this case, SWs with a homogeneous profile along the nanotube long axis propagate only in the azimuthal direction with wavenumber n . Since the propagation direction and the magnetization are parallel, this case resembles the BV geometry of the SW propagation in planar thin films. The frequency linewidth takes the form

$$\Gamma(n, 0) = \alpha_G \omega_{M_s} ((2n^2 - 1)h_u + 2h_0 + \mathcal{J}_0^n), \quad (20)$$

which for the exchange-dominated regime, i.e., $n \gg 1$, is written as

$$\Gamma(n \gg 1, 0) = \omega_{M_s} \alpha_G \left(2n^2 h_u + 2h_0 + \frac{1}{n} \frac{R^2 + r^2}{R^2 - r^2} \right). \quad (21)$$

For nanotubes with a radius much larger than the thickness $R \gg d$, the previous equation can be written as

$$\Gamma(n \gg 1, 0) = \omega_{M_s} \alpha_G \left(2l_{ex}^2 \bar{k}_\varphi^2 + 2h_0 + \frac{1}{\bar{k}_\varphi d} \right), \quad (22)$$

where d is the nanotube thickness. Equation 22 is similar to the expression of the linewidth that one can obtain for 2D thin films for the BV modes. In the case of zero azimuthal wavenumber $n = 0$ (typically called the ferromagnetic resonance (FMR) mode), the frequency linewidth is

$$\Gamma(0, 0) = \alpha_G \omega_{M_s} (2h_0 - h_u + 1), \quad (23)$$

which resembles the FMR frequency linewidth known from the Kittel formula³² for a thin film with a homogeneous in-plane magnetization parallel to the applied magnetic field H_0 .

B. For $k_z \gg 1/R$

In this case, the SW wavelength is considerably smaller than the nanotube radius. Therefore, the SWs are exchange dominated, and the dispersion relation is symmetric. The frequency linewidth can be written as

$$\Gamma(n, k_z \gg 1/R) = \alpha_G \omega_{M_s} (2l_{ex}^2 k_z^2 + (2n^2 - 1)h_u + 2h_0 + 1). \quad (24)$$

For $n = 0$ or SWs with no nodal lines, equation 24 resembles the linewidth of Damon-Eshbach (DE) modes in 2D thin films with in-plane magnetization (see equation 19).

C. For $k_z \neq 0$ ($k_z \ll 1/R$)

As the last case, the linewidth of SWs with small wavevectors is discussed. At this limit, the hyperfunctions shown in equation 7 can be approximated as shown

$$\Gamma(n, k_z \ll 1/R) \approx \alpha_G \omega_{M_s} \left((2l_{ex}^2 + w_n - u_n)k_z^2 + (2n^2 - 1)h_u + 2h_0 + 1 \right) \times \left(1 + \frac{\nu_n k_z}{\sqrt{((l_{ex}^2 + w_n)k_z^2 + (n^2 - 1)h_u + h_0)((l_{ex}^2 - u_n)k_z^2 + n^2h_u + h_0 + 1)}} \right) \quad (25)$$

where ν_n , u_n and w_n can only be calculated numerically (for details, see Ref.²³). However, these coefficients were

in Otálora *et al.*²³, resulting in $\mathcal{A}_{k_z}^0 \approx \nu_n k_z$, $\mathcal{J}_{k_z}^0 \approx (1 - u_n)k_z^2$ and $\mathcal{L}_{k_z}^0 \approx (1 - w_n)k_z^2$. Therefore, the frequency linewidth will have the following complex expression:

already calculated for $n = 0$ (see figure 7 in Ref.²³), and for this particular case, the frequency linewidth takes the form

$$\Gamma(0, k_z \ll 1/R) \approx \alpha_G \omega_{M_s} \left((2l_{ex}^2 + w - u)k_z^2 - h_u + 2h_0 + 1 \right) \times \left(1 + \frac{\nu_0 k_z}{\sqrt{((l_{ex}^2 + w_0)k_z^2 - h_u + h_0)((l_{ex}^2 - u_0)k_z^2 + h_0 + 1)}} \right). \quad (26)$$

Equation 26 shows that the asymmetry is linear in k_z for counterpropagating SWs. It can be observed by taking into account the change in the sign of k_z for opposite propagations. Note that the curvature-induced asymmetries in the frequency linewidth are similar to those obtained for heavy metal/magnetic metal 2D sandwiches with interfacial DMI for SWs in the DE configuration. In Ref.¹⁷, a similar linear term, originating from the interfacial DMI, appears in the frequency linewidth expression.

VI. CONCLUSIONS

We have elaborated an analytical model of the frequency linewidth for curved magnetic membranes with a tubular geometry. It is found that the linewidth is asymmetric regarding the eigenfrequency of the SWs and the sign of the propagation vector. The asymmetry originates from the dynamic dipolar fields and is directly related to the mean curvature of the magnetic nanotube. In contrast to the 2D thin film, for SWs in the DE geometry, the dynamic dipolar fields produce an extra contribution that is linear in k in the linewidth. Consequently, SWs propagating to opposite directions but with the same frequency have different lifetimes, group velocities and thus different decay lengths. The predicted asymmetry of the linewidth shows a similar tendency as that reported for the dispersion relation of the nanotubes in our previous works^{22,23}. We also show that the asymmetries presented in the group velocity and frequency linewidth lead to a decay length with evident asymmetries, which is also

calculated. Indeed, changes between 10% and 20% in frequency linewidth and between 10% and 22% in the decay length for counterpropagating SWs are predicted. Furthermore, it is shown that for modes with azimuthal wavevector only ($k_z = 0$) and large radius, the expression of the linewidth reduced to a formula similar to that of the BV modes in planar thin films. In the limiting case of SWs with a wavelength that is considerably smaller than the nanotube radius ($k_z \gg 1/R$) and no nodal lines (higher-order modes excluded: $n = 0$), the linewidth resembles the linewidth that one obtains for the DE modes in planar thin films. Finally, in the last case for intermediate SW wavelengths $k_z \neq 0$ ($k_z \ll 1/R$), the obtained expression for the linewidth is similar to that obtained for heavy metal/magnetic metal 2D sandwiches with interfacial DMI for SWs in the DE configuration. However, the linear term responsible for the asymmetry originates from the dynamic volume changes. We believe that our findings represent a step forward toward the realization of 3D curvilinear magnonic devices.

ACKNOWLEDGMENTS

Fruitful discussions with Kai Wagner are acknowledged.

AUTHOR CONTRIBUTIONS

J.A.O. developed the analytical model and wrote the manuscript. All authors interpreted and discussed the results and co-wrote the manuscript.

ADDITIONAL INFORMATION

The authors declare no competing financial interests. Reprints and permission information is available online at <http://XXXXXX>. Correspondence and requests for materials should be addressed to J.A.O.

REFERENCES

- ¹F. Bloch, *Zeitschrift für Physik* **61**, 206 (1930).
- ²D. Grundler, *Nat Phys* **11**, 438 (2015).
- ³D. Grundler, *Nature nanotechnology* (2016).
- ⁴A. V. Chumak, V. I. Vasyuchka, A. A. Serga, and B. Hillebrands, *Nat Phys* **11**, 453 (2015).
- ⁵K. Vogt, H. Schultheiss, S. Jain, J. E. Pearson, A. Hoffmann, S. D. Bader, and B. Hillebrands, *Applied Physics Letters* **101**, 042410 (2012), <http://dx.doi.org/10.1063/1.4738887>.
- ⁶A. V. Chumak, A. A. Serga, and B. Hillebrands, *Nat Commun* **5** (2014).
- ⁷K. Vogt, F. Y. Fradin, J. E. Pearson, T. Sebastian, S. D. Bader, B. Hillebrands, A. Hoffmann, and H. Schultheiss, *Nat Commun* **5** (2014).
- ⁸B. Lenk, H. Ulrichs, F. Garbs, and M. Münzenberg, *Phys. Rep.* **507**, 107 (2011).
- ⁹J. Otálora, D. Cortés-Ortuño, D. Görlitz, K. Nielsch, and P. Landeros, *Journal of Applied Physics* **117**, 173914 (2015).
- ¹⁰A. V. Chumak, A. A. Serga, and B. Hillebrands, *Nature communications* **5** (2014).
- ¹¹A. Chumak, V. Vasyuchka, A. Serga, and B. Hillebrands, *Nature Physics* **11**, 453 (2015).
- ¹²I. Dzyaloshinsky, *Journal of Physics and Chemistry of Solids* **4**, 241 (1958).
- ¹³T. Moriya, *Physical Review* **120**, 91 (1960).
- ¹⁴K. Zakeri, Y. Zhang, J. Prokop, T.-H. Chuang, N. Sakr, W. X. Tang, and J. Kirschner, *Physical Review Letters* **104**, 137203 (2010).
- ¹⁵D. Cortés-Ortuño and P. Landeros, *Journal of Physics: Condensed Matter* **25**, 156001 (2013).
- ¹⁶F. Ma and Y. Zhou, *RSC Adv.* **4**, 46454 (2014).
- ¹⁷K. Di, V. L. Zhang, H. S. Lim, S. C. Ng, M. H. Kuok, J. Yu, J. Yoon, X. Qiu, and H. Yang, *Physical review letters* **114**, 047201 (2015).
- ¹⁸Y. Iguchi, S. Uemura, K. Ueno, and Y. Onose, *Phys. Rev. B* **92**, 184419 (2015).
- ¹⁹R. Hertel, *SPIN* **3**, 1340009 (2013).
- ²⁰Y. Gaididei, A. Goussev, V. P. Kravchuk, O. V. Pylypovskiy, J. Robbins, D. D. Sheka, V. Slastikov, and S. Vasylykevych, arXiv preprint arXiv:1701.01691 (2017).
- ²¹D. D. Sheka, V. P. Kravchuk, K. V. Yershov, and Y. Gaididei, *Phys. Rev. B* **92**, 054417 (2015).
- ²²J. A. Otálora, M. Yan, H. Schultheiss, R. Hertel, and A. Kákay, *Physical review letters* **117**, 227203 (2016).
- ²³J. A. Otálora, M. Yan, H. Schultheiss, R. Hertel, and A. Kákay, *Phys. Rev. B* **95**, 184415 (2017).
- ²⁴D. Polder, *The London, Edinburgh, and Dublin Philosophical Magazine and Journal of Science* **40**, 99 (1949).
- ²⁵M. Hurben and C. Patton, *Journal of Applied Physics* **83**, 4344 (1998).
- ²⁶R. Arias and D. L. Mills, *Phys. Rev. B* **60**, 7395 (1999).
- ²⁷P. Landeros, R. E. Arias, and D. Mills, *Physical Review B* **77**, 214405 (2008).
- ²⁸R. Gallardo, A. Banholzer, K. Wagner, M. Körner, K. Lenz, M. Farle, J. Lindner, J. Fassbender, and P. Landeros, *New Journal of Physics* **16**, 023015 (2014).
- ²⁹D. Twisselmann and R. D. McMichael, *Journal of Applied Physics* **93**, 6903 (2003).
- ³⁰S. S. Kalarickal, P. Krivosik, M. Wu, C. E. Patton, M. L. Schneider, P. Kabos, T. J. Silva, and J. P. Nibarger, *Journal of Applied Physics* **99**, 093909 (2006).
- ³¹Note that the same stiffness fields appear in the dispersion relation $(\omega_{2D}[\vec{k}] = \omega_{M_s} \sqrt{h_X[\vec{k}]h_Y[\vec{k}]})$.
- ³²C. Kittel, *Introduction to Solid State Physics*, 6th ed. (John Wiley & Sons, Inc., New York, 1986).